

Neutrino Parameters from Reactor and Accelerator Neutrino Experiments

Manfred Lindner, Werner Rodejohann and Xun-Jie Xu

Max-Planck-Institut für Kernphysik, Postfach 103980, D-69029 Heidelberg, Germany

(Dated: December 14, 2024)

We revisit correlations of neutrino oscillation parameters in reactor and long-baseline neutrino oscillation experiments. A framework based on an effective value of θ_{13} is presented, which can easily reproduce experimental results. It also clarifies why current and future long-baseline experiments will have less precision on values around $\delta_{CP} = \pm\pi/2$ than on values around $\delta_{CP} = 0$. Optimization potential for the determination of the theoretically very interesting values around $\delta_{CP} = -\pi/2$ is also pointed out, which would require that future runs of accelerator experiments are not equally shared 1 : 1 in neutrino and antineutrino modes, but rather 2 : 1. Recent hints on the CP phase and the mass ordering are then considered from the point of view that different reactor and long-baseline neutrino experiments provide currently different best-fit values of θ_{13} and θ_{23} . We point out that the significance of the hints changes for the different available best-fit values.

I. INTRODUCTION

Short-baseline reactor and long-baseline accelerator neutrino experiments are of huge importance in the era of neutrino oscillation precision measurements. The precision determination of θ_{23} , and the measurements of the CP phase δ_{CP} and the neutrino mass ordering would help further understanding the leptonic flavor sector and could bring various insights in models behind neutrino mass and lepton mixing.

The interplay of long- and short-baseline experiments is exemplified by the dependence of the electron antineutrino survival probability in reactor experiments, which depends on θ_{13} , and the $\nu_\mu \rightarrow \nu_e$ (or $\bar{\nu}_\mu \rightarrow \bar{\nu}_e$) transition probability in accelerator experiments, which depends on θ_{13} , θ_{23} , δ_{CP} and the mass ordering. Inserting the reactor determination of θ_{13} , as well as θ_{23} values from atmospheric data or long-baseline muon neutrino survival probabilities, into $\nu_\mu \rightarrow \nu_e$ (or $\bar{\nu}_\mu \rightarrow \bar{\nu}_e$) measurements can give hints on the CP phase [1, 2]. Combining $\nu_\mu \rightarrow \nu_e$ plus $\bar{\nu}_\mu \rightarrow \bar{\nu}_e$ data with additional input on θ_{23} is enough to get sensitivity on δ_{CP} [3, 4]. As matter effects start to play a non-negligible role also some sensitivity on the mass ordering can occur by combining different data sets. Indeed, recently hints towards non-trivial values of the CP phase δ_{CP} and some preference of the normal ordering over the inverted one were found in combining short-baseline reactor and long-baseline accelerator neutrino experiments, see Refs. [5–7] for recent global fits.

In this respect, one should note here the different values of θ_{13} that have been determined by the three reactor neutrino experiments: $\theta_{13} = 8.43^\circ_{-0.17}^{+0.17}$ (Daya Bay [8]), $8.62^\circ_{-0.57}^{+0.54}$ (RENO [9]) and $9.73^\circ_{-0.85}^{+0.79}$ (Double Chooz [10]). It is possible that the central value of θ_{13} is shifted (e.g. from a joint analysis of the collaborations), which will then have consequences on the determination of the other neutrino parameters. Moreover, the best-fit values (normal ordering for definiteness) of θ_{23} are 46.8° from T2K [11] and 39.5° (52.2°) from NO ν A [12], where the latter has two almost equally good best-fit points. In this paper we try to estimate the possible impact of the different central values of θ_{13} and θ_{23} on the hints for CP violation and the normal mass ordering. Towards this end, we re-analyze the correlation of long-baseline $\nu_\mu \rightarrow \nu_e$ ($\bar{\nu}_\mu \rightarrow \bar{\nu}_e$) transition and reactor $\bar{\nu}_e \rightarrow \bar{\nu}_e$ survival oscillations. The concept of an “effective” θ_{13}^{eff} is introduced, which is the quantity on which accelerator experiments are only sensitive to, and which can be compared to the “naked” θ_{13} which is determined in reactor experiments. This formalism can easily explain why future long-baseline experiments will have less precision on values around $\delta_{CP} = \pm\pi/2$ than on values around $\delta_{CP} = 0$.

Focusing on the for phenomenologists easier to reproduce T2K data (and not using in particular the far more difficult to reproduce atmospheric neutrino data), we show that by applying θ_{13}^{eff} the results on the oscillation parameters from the experiment can be reproduced with very good accuracy. The formalism clarifies why current and future long-baseline experiments will have less precision on values around $\delta_{CP} = \pm\pi/2$ than on values around $\delta_{CP} = 0$. We study the impact of combining accelerator neutrino data with antineutrino data, and with reactor data. We investigate the impact of the different θ_{13} and θ_{23} best-fit values on the determination of δ_{CP} , as well as on the preference for the normal mass ordering. We demonstrate that the significance can shift, and should thus be taken with care. For instance, the preference for the normal mass ordering from appearance data may be reduced by more than one standard deviation. We also remark that the theoretically very interesting value of $\delta_{CP} = -\pi/2$ can be measured with currently running accelerator experiments better if future runs are not equally shared 1 : 1 in neutrino and antineutrino modes, but rather 2 : 1.

The remainder of this paper is organized as follows. In Sec. II we introduce the effective θ_{13}^{eff} for accelerator neutrino experiments as well as investigate the accuracy of this framework when neutrino parameters are determined. The

actual derivation of θ_{13}^{eff} is performed in Sec. III, where also the sensitivity of long-baseline experiments to the CP phase is discussed. In Sec. IV, we turn to phenomenological studies, including the impact of the different available central values of θ_{13} and θ_{23} on the CP phase δ_{CP} and the mass ordering. Finally, we summarize in Sec. V.

II. EFFECTIVE θ_{13}

We start from the approximate neutrino oscillation formula [13–15] that can accurately describe $\nu_\mu \rightarrow \nu_e$ transitions in current and upcoming accelerator neutrino experiments such as T2K [1, 16], MINOS [17], NO ν A [18, 19], DUNE [20] or T2HK [21]:

$$\begin{aligned} P(\nu_\mu \rightarrow \nu_e) \approx & 4s_{13}^2 c_{13}^2 s_{23}^2 \frac{\sin^2(1-A)\Delta}{(1-A)^2} \\ & - 8\alpha J_{CP} \sin \Delta \frac{\sin A\Delta}{A} \frac{\sin(1-A)\Delta}{1-A} \\ & + 8\alpha (J_{CP} \cot \delta_{CP}) \cos \Delta \frac{\sin A\Delta}{A} \frac{\sin(1-A)\Delta}{1-A} \\ & + 4\alpha^2 s_{12}^2 c_{12}^2 c_{23}^2 \frac{\sin^2 A\Delta}{A^2}. \end{aligned} \quad (1)$$

Here $(s_{ij}, c_{ij}) \equiv (\sin \theta_{ij}, \cos \theta_{ij})$, $\alpha \equiv \Delta m_{21}^2 / \Delta m_{31}^2$, $A \equiv 2\sqrt{2}G_F N_e E / \Delta m_{32}^2$ (N_e is the electron number density in matter), $\Delta \equiv \Delta m_{32}^2 L / (4E)$ and

$$J_{CP} = \frac{1}{8} \sin \delta_{CP} \sin 2\theta_{12} \sin 2\theta_{13} \sin 2\theta_{23} c_{13}. \quad (2)$$

The matter effect [22–24] is included by the parameter A . For $\bar{\nu}_\mu \rightarrow \bar{\nu}_e$ transitions, Eq. (1) can be used by replacing $\delta_{CP} \rightarrow -\delta_{CP}$ (implying $J_{CP} \rightarrow -J_{CP}$) and $A \rightarrow -A$. For the two possibilities of the mass ordering, namely the normal/inverted ordering (NO/IO), the formula allows negative Δm_{32}^2 , i.e. in the IO one takes negative values of A , α and Δ . Eq. (1) is derived from the series expansion in α where the leading order (LO), next-to-leading order (NLO), and next-to-next-to leading order (NNLO) terms correspond to the first, second plus third, and last rows of Eq. (1), respectively¹. At LO, the oscillation probability of $\nu_\mu \rightarrow \nu_e$ depends on θ_{13} and θ_{23} , but is independent of δ_{CP} , which appears at NLO.

Let us first focus on the LO and neglect the higher order terms so Eq. (1) can be approximately written as

$$P(\nu_\mu \rightarrow \nu_e) \approx \frac{1}{2} \sin^2 2\theta_{13}^{\text{eff}} \frac{\sin^2(1-A)\Delta}{(1-A)^2}, \quad (3)$$

where

$$\sin^2 2\theta_{13}^{\text{eff}} = 2s_{23}^2 \sin^2 2\theta_{13} + \mathcal{O}(\alpha). \quad (4)$$

Here we have introduced an angle θ_{13}^{eff} which we will refer to as *effective* θ_{13} in this paper. At this stage it is only the coefficient $4s_{13}^2 c_{13}^2 s_{23}^2$ of the LO expression, but below we will further generalize it to higher orders and provide a more general definition. Note that in the limit $\alpha \rightarrow 0$ and $\theta_{23} \rightarrow 45^\circ$, θ_{13}^{eff} is equal to θ_{13} . At this level a correlation exists only with θ_{23} and θ_{13} . For a given set of ν_e appearance data, if the input value of θ_{23} is increased then the output value of θ_{13} will be decreased.

Generalizing the definition of θ_{13}^{eff} by including higher order terms will be more complicated since the NLO and NNLO terms have different energy dependence. The spectrum of the neutrino beam and the efficiency of neutrino detection have to be involved. Hence, any generalization will be experiment-dependent. We postpone these experimental details to the next section and simply present the result here. According to the analysis in Sec. III, we find that θ_{13}^{eff} can be generalized to NLO and NNLO as follows:

$$\frac{1}{2} \sin^2 2\theta_{13}^{\text{eff}} \equiv s_{23}^2 \sin^2 2\theta_{13} - 8\alpha J_{CP} f_s + 8\alpha \frac{J_{CP}}{\tan \delta_{CP}} f_c + \alpha^2 \sin^2 2\theta_{12} c_{23}^2 f_2. \quad (5)$$

¹ More exactly, the accuracy requires not only small α , but also small $\alpha\Delta$, s_{13}^2 , etc. See Ref. [25] for a detailed discussion on the validity of Eq. (1).

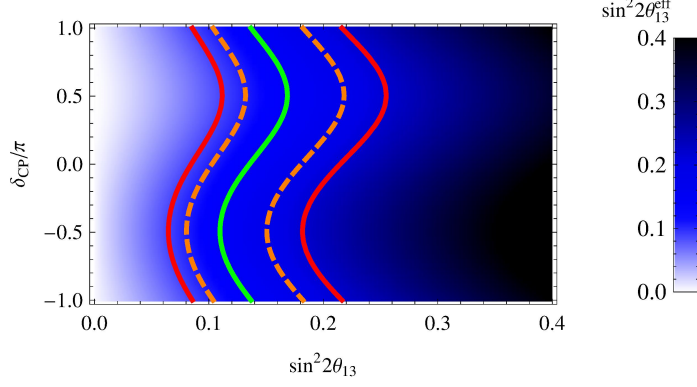


Figure 1. Contour plot of $\sin^2 2\theta_{13}^{\text{eff}}(\theta_{13}, \delta_{CP})$ for the normal mass ordering. The five contours from the left to the right correspond to $\sin^2 2\theta_{13}^{\text{eff}} = 0.087, 0.106, 0.139, 0.184$ and 0.218 , respectively. Normal mass ordering is assumed, with $(\theta_{12}, \theta_{23}, \alpha) = (34^\circ, 45^\circ, 0.031)$.

Here f_s , f_c and f_2 are numerical factors depending on the experimental configurations, including baseline, neutrino beam, detector, etc. For example, in T2K, assuming normal mass hierarchy, from the calculations in Sec. III we have

$$f_s^{\text{T2K}} = 1.42083, f_c^{\text{T2K}} = 0.0314521, f_2^{\text{T2K}} = 2.98237. \quad (6)$$

It turns out that in actual accelerator neutrino experiments one can use Eq. (3), with θ_{13}^{eff} defined in Eq. (5), to compute the distribution of events very accurately. The small difference to Eq. (1) is negligible in practice.

To sum up so far, only θ_{13}^{eff} is measurable in $\nu_\mu \rightarrow \nu_e$ transitions in an accelerator neutrino experiment. All correlations among the PMNS parameters θ_{13} , θ_{23} and δ_{CP} in $\nu_\mu \rightarrow \nu_e$ transitions are included in Eq. (5).

Using the values from Eq. (6) and the best-fit values [6] of θ_{23} , θ_{12} and α , we can draw a contour plot of $\sin^2 2\theta_{13}^{\text{eff}}(\theta_{13}, \delta_{CP})$, as shown in Fig. 1. We choose five different values for $\sin^2 2\theta_{13}^{\text{eff}}$ and plot the corresponding contours. As one can see from these contours, they all appear in the shape of sine curves, which originates of course from the CP -odd term (the second term) in Eq. (5) that contains $\sin \delta_{CP}$. The CP -even term can be neglected because f_c^{T2K} is very small (see next section).

Fig. 1 implies that for a fixed value of θ_{13}^{eff} , θ_{13} approximately increases with $\sin \delta_{CP}$; it reaches the maximum (minimum) when δ_{CP} is close to $\pi/2$ ($-\pi/2$). As a consequence, if θ_{13}^{eff} measured in T2K is larger² than the measured reactor neutrino value of θ_{13} , the favored value of δ_{CP} in the combined analysis will necessarily be about $-\pi/2$.

Moreover, the shape of the contours resembles the constraint on $(\theta_{13}, \delta_{CP})$ published by the T2K collaboration (cf. Fig. 5 in Ref. [1], Fig. 39 in Ref. [4], or Fig. 2 in this paper). Indeed, since the actual observable in such experiments is $\sin^2 2\theta_{13}^{\text{eff}}$ which contains $(\theta_{13}, \delta_{CP})$, the constraint on $(\theta_{13}, \delta_{CP})$ can be readily reproduced, given the T2K constraint on $\sin^2 2\theta_{13}^{\text{eff}}$. Fig. 2 shows the reproduced constraint based on our effective θ_{13} framework, compared with the original constraint in Ref. [4]. The results agree very well with each other, which implies that our effective θ_{13} framework is able to quantitatively describe the sensitivity of T2K $\nu_\mu \rightarrow \nu_e$ data on $(\theta_{13}, \delta_{CP})$ with sufficient accuracy. The details of reproducing the constraint are given next.

Since the expected event number μ should linearly depend on the probability of ν_e appearance, it should also linearly depend on $S^2 \equiv \sin^2 2\theta_{13}^{\text{eff}}$. So we can write

$$\mu = kS^2 + b, \quad (7)$$

where k is a scale factor and b can be regarded as the background because it equals the expected event number without neutrino oscillation. The observed event number n should obey a Poisson distribution, hence the χ^2 -function of μ is

$$\chi^2(\mu) = 2 \left(\mu - n + n \ln \frac{n}{\mu} \right). \quad (8)$$

² Since the T2K value of θ_{13}^{eff} is CP -dependent, here “larger” means for any value of δ_{CP} it is always larger than the reactor value.

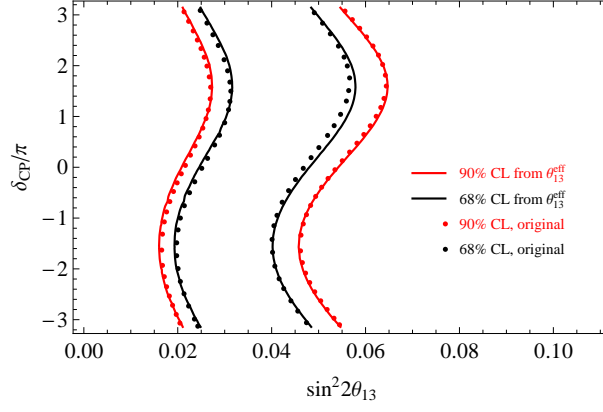


Figure 2. Reproduced constraints (red and black curves) on $(\theta_{13}, \delta_{CP})$ from our effective θ_{13} framework compared to the original T2K result [4] (red and black points) for the normal mass ordering. The agreement shows that the effective θ_{13} framework is very accurate to describe the sensitivity of T2K $\nu_\mu \rightarrow \nu_e$ data on $(\theta_{13}, \delta_{CP})$.

By plugging Eq. (7) into Eq. (8) we obtain the χ^2 -function of S^2 ,

$$\chi^2(S^2) = 2 \left(kS^2 + b - n + n \ln \frac{n}{kS^2 + b} \right). \quad (9)$$

For the T2K ν_e appearance data, so far the observed event number n is 32; the two parameters k and b can be determined by comparing Eq. (9) to the original T2K result [4], which gives $(k, b) = (1.86 \times 10^2, 4.84)$. We have here extracted k and b from Fig. 39 of Ref. [4]. Eq. (9) can be further converted to the χ^2 -function of $(\theta_{13}, \delta_{CP})$ if α , θ_{23} and θ_{12} are fixed or marginalized over. In Fig. 2 we simply use fixed values $\alpha = 0.0307$, $\theta_{23} = 46.5^\circ$ and $\theta_{12} = 33.4^\circ$ to generate the black and red curves. Although the original T2K result was obtained by marginalizing all nuisance parameters, our result using fixed values already agrees well with it.

III. EVALUATING THE f -FACTORS

In this section we will derive the effective θ_{13}^{eff} including the experiment-dependent values f_s , f_c and f_2 , see Eq. (5). We start by writing the observable event rate in a neutrino experiment as follows:

$$\frac{dN}{d\Omega_f} = \Delta t \int D(E_\nu, \Omega_f) P(E_\nu) \Phi(E_\nu) dE_\nu, \quad (10)$$

Here Ω_f includes final states of all observable particles after scattering (e.g. energy/momentum of an electron), Δt is the time of exposure, and (Φ, P, D) represent functions describing neutrino production, propagation and detection, respectively. More explicitly, Φ is the flux of neutrinos produced at the source, P is the oscillation probability during propagation, and D is defined as the probability of an incoming neutrino causing an event in which the final states are given by Ω_f . Basically, D is the differential cross section but practically it should also include the efficiency of detecting final state particles (e.g. detecting photons in PMTs).

Integrating with respect to Ω_f in Eq. (10), one can obtain the total event number. To understand the contribution of each term in Eq. (1) we decompose it into four terms:

$$P = P_0 + P_s + P_c + P_2. \quad (11)$$

Here the four terms are

$$P_0(E_\nu) \equiv 4s_{13}^2 c_{13}^2 s_{23}^2 p_0(E_\nu), \quad (12)$$

$$P_s(E_\nu) \equiv -8\alpha J_{CP} p_s(E_\nu), \quad (13)$$

$$P_c(E_\nu) \equiv 8\alpha J_{CP} \cot \delta_{CP} p_c(E_\nu), \quad (14)$$

$$P_2(E_\nu) \equiv 4\alpha^2 s_{12}^2 c_{12}^2 c_{23}^2 p_2(E_\nu), \quad (15)$$

where the energy-dependent parts are defined as

$$p_0 \equiv \frac{\sin^2(1-A)\Delta}{(1-A)^2}, \quad (16)$$

$$p_s \equiv \sin \Delta \frac{\sin A \Delta}{A} \frac{\sin(1-A)\Delta}{1-A}, \quad (17)$$

$$p_c \equiv \cos \Delta \frac{\sin A \Delta}{A} \frac{\sin(1-A)\Delta}{1-A}, \quad (18)$$

$$p_2 \equiv \frac{\sin^2 A \Delta}{A^2}. \quad (19)$$

In the integral, we are only concerned about the energy-dependent parts of P so we define

$$N_X \equiv \Delta t \int \left(\int D d\Omega_f \right) p_X \Phi dE_\nu, \text{ for } X = 0, s, c, 2. \quad (20)$$

Then the total event number will be

$$N_{\text{tot}} = s_{23}^2 \sin^2 2\theta_{13} N_0 - 8\alpha J_{CP} N_s + 8\alpha \frac{J_{CP}}{\tan \delta_{CP}} N_c + \alpha^2 \sin^2 2\theta_{12} c_{23}^2 N_2. \quad (21)$$

As we can see from Eq. (21), by introducing $N_{0,s,c,2}$, the dependence of the total event number on the PMNS parameters is explicitly kept. The f -factors introduced in the effective θ_{13}^{eff} in Eq. (5) are defined as

$$(f_s, f_c, f_2) \equiv \frac{(N_s, N_c, N_2)}{N_0}, \quad (22)$$

which shows that they are the contributions of the different oscillation modes p_s, p_c and p_2 to the total event number, in comparison to the dominant mode p_0 . Since Eq. (22) is a ratio, all overall factors (such as Δt) will be canceled in Eq. (22). In practice the f -factors can thus be evaluated by

$$f_X = \frac{\int F(E_\nu) p_X(E_\nu) dE_\nu}{\int F(E_\nu) p_0(E_\nu) dE_\nu}, \text{ for } X = s, c, 2, \quad (23)$$

where

$$F(E_\nu) \equiv \left(\int D(E_\nu, \Omega_f) d\Omega_f \right) \Phi(E_\nu). \quad (24)$$

If one disregards the efficiency of detecting final state particles (assuming it is 100% or an energy-independent constant), then the integral in Eq. (24) can be replaced with the total cross section $\sigma(E_\nu)$. Therefore we have

$$F(E_\nu) \propto \sigma(E_\nu) \Phi(E_\nu). \quad (25)$$

So far the discussion was general. Let us take now the $\nu_\mu \rightarrow \nu_e$ measurement of T2K as an example and evaluate the f -factors. The T2K experiment uses an off-axis beam of muon neutrinos generated at the J-PARC accelerator in Tokai, Japan. For $\Phi(E_\nu)$ in Eq. (25), we take the ν_μ flux from Ref. [26]. The Super-Kamiokande (SK) far detector (295 km away from the source) is a water Cherenkov detector in which neutrinos are detected via Cherenkov light of charged particles emitted from neutrino scattering. Since the selected ν_e events are expected from charged current quasi-elastic (CCQE) scattering, we only need the CCQE cross section for $\sigma(E_\nu)$ in Eq. (25). In water (H_2O , where we only consider ^{16}O) we use the CCQE cross section data from GENIE [27]. Given the cross section and the neutrino flux, we can compute $F(E_\nu)$ in Eq. (25), up to an irrelevant normalization factor. The shape of $F(E_\nu)$ is presented in Fig. 3.

Next we compute the integrals in Eq. (23) with $G_F N_e = 7.01 \times 10^{-14} \text{ eV}$ (corresponding to the terrestrial matter density $\rho = 1.3 \text{ g/cm}^3$) and $|\Delta m_{31}^2| = 2.44 \times 10^{-3} \text{ eV}^2$. The numerical results are listed in Tab. I, including both ν_e and $\bar{\nu}_e$ modes, NO and IO. For IO, one should use negative Δm_{31}^2 so Δ and A are negative, leading to a negative f_s . For the $\bar{\nu}_e$ mode, one should change the neutrino flux and cross section correspondingly, and flip the signs of A and δ_{CP} , which means the negative sign before the second term of Eq. (1) should change to positive. Since we want a unified definition of θ_{13}^{eff} for both ν_e and $\bar{\nu}_e$ [i.e. the form of Eq. (10) should also apply to $\bar{\nu}_e$], we add a negative sign in p_s for the $\bar{\nu}_e$ mode. As a consequence, f_s for $\bar{\nu}_e$ with NO or IO is negative or positive, respectively.

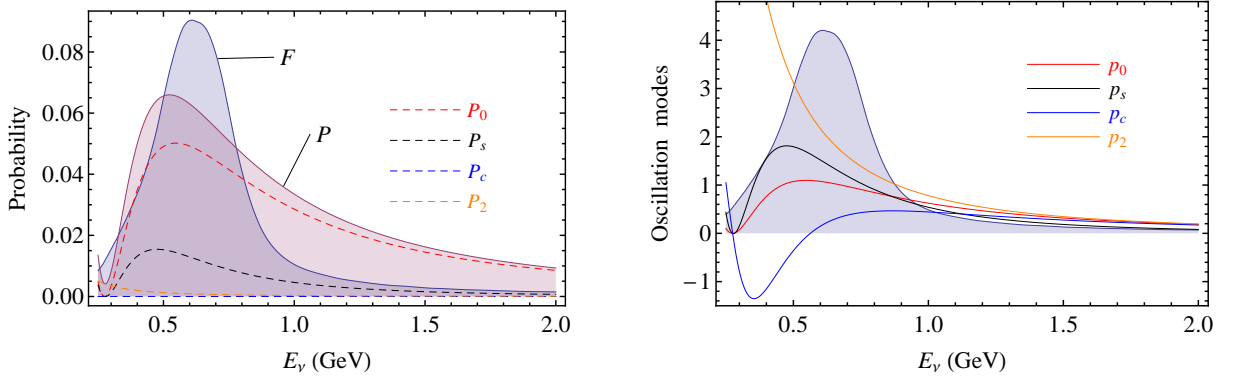


Figure 3. The probability of $\nu_\mu \rightarrow \nu_e$ transitions and $F(E_\nu)$ in T2K [cf. Eqs. (11) and (25)]. The definitions of P_X and p_X ($X = 0, s, c, 2$) are given in Eqs. (12) to (19), P is the total oscillation probability for $(\theta_{23}, \theta_{13}, \theta_{12}) = (45^\circ, 8.8^\circ, 34^\circ)$, $\Delta m_{13}^2 = 2.44 \times 10^{-3} \text{ eV}^2$, $\alpha = 0.31$, and $\delta_{CP} = -\pi/2$ (hence $P_c = 0$). The function F is presented in arbitrary units.

Table I. The f factors in T2K.

	ν_e normal	ν_e inverted	$\bar{\nu}_e$ normal	$\bar{\nu}_e$ inverted
f_s	1.42083	-1.62128	-1.52638	1.47037
f_c	0.0314521	-0.0159949	0.107811	-0.0327648
f_2	2.98237	4.04585	3.51664	3.30968

Note that f_c^{T2K} is much smaller than f_s^{T2K} which implies that at NLO the CP -even term in Eq. (1) has a much smaller contribution to the oscillation probability than the CP -odd term. Let us discuss the physical meaning of the f -factors to understand why f_c^{T2K} is so small. As shown in Fig. 3, the function $F(E_\nu)$ which is proportional to both the detection rate D and the flux Φ , peaks at about 0.6 GeV but is suppressed at both high and low energies. This is because if E_ν is too high, the flux drops exponentially; if E_ν is too low, the cross section suppresses F (the flux drops as well). On the other hand, the oscillation probability P also shows similar dependence on E_ν (if one only focuses on the dominating first peak of oscillation). Therefore, in order to obtain sizable event numbers, it is important to make F (which is essentially flux times cross section) and the probability P overlap as much as possible when they obtain their maximal values.

In the left panel of Fig. 3, we show the contribution of each term of the probability, i.e. P_0 , P_s , P_c and P_2 [cf. Eqs. (11)-(15)]. In the right panel, we focus on the pure oscillation modes, p_0 , p_s , p_c and p_2 [cf. Eqs. (16)-(19)] which are directly related to the f -factors according to Eq. (23). The physical meaning of f_X ($X = s, c, 2$) is how much the corresponding oscillation mode p_X and the function $F(E_\nu)$ overlap, which determines the sensitivity of the experiment on this mode itself. As we can see, p_c has the least overlap with the shaded region corresponding to F , and it also contains a negative part which causes cancellation with the positive part. This explains why f_c is much smaller than the other f -factors.

Although the smallness of f_c is experiment dependent, it should be a general feature in accelerator neutrino experiments because usually the experiments should be designed so that $F(E_\nu)$ peaks at the same energy where the oscillation mode $\sin^2 \Delta$ peaks. The oscillating part in p_c [cf. (18)] approximates in the valid limit of small matter effects as $\sin \Delta \cos \Delta$, which if integrated with the function F (see Fig. 3) will always lead to the similar cancellation. Therefore one can conclude that in general f_c is small in such experiments. As a consequence of small f_c , the CP -even contribution (defined by the events generated by the oscillation term proportional to $\cos \delta_{CP}$) is small, which makes the measurement of δ_{CP} in the experiments such as T2K and DUNE actually sensitive to $\sin \delta_{CP}$ rather than $\cos \delta_{CP}$. This also explains why the uncertainties of δ_{CP} in future measurements will be maximal or minimal if the true value of δ_{CP} is $\pm 90^\circ$ or 0, respectively—see, e.g., Refs. [28–30].

Finally, we would like to discuss the validity of the effective θ_{13}^{eff} when applied to accelerator neutrino experiments. When introducing the effective θ_{13}^{eff} , we actually assume that the observable effects of the NLO and NNLO terms are only their contributions to the total event number, i.e. the distortion of the shape of $\nu_e(\bar{\nu}_e)$ distribution due to the different oscillation modes is assumed to be negligible. However, for experiments with very high sensitivities, this assumption might not hold. To understand the differences between the effective θ_{13} and the conventional treatment, we compare the event rates in Fig. 4. The event rates are plotted in arbitrary units, computed via $F(E_\nu) \times P(E_\nu)$ where $P(E_\nu)$ takes either the form of Eq. (3) [with θ_{13}^{eff} defined in (5)] or of Eq. (1), plotted by the blue dashed or the black solid curve, respectively. From Fig. 4 we can see that the difference between the two curves is very

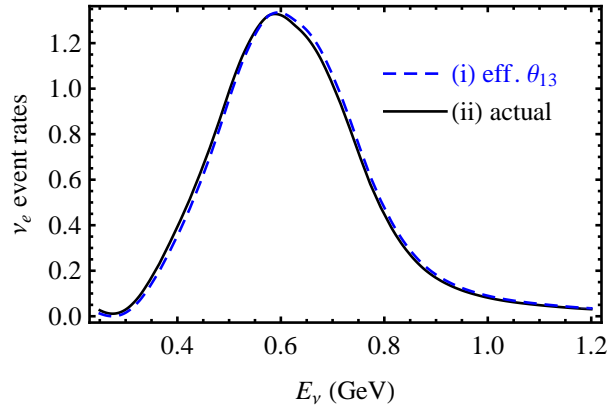


Figure 4. Comparison of ν_e event rates (in arbitrary units) computed (i) from the effective θ_{13}^{eff} formula [cf. Eqs. (3) and (5)] and (ii) from the actual oscillation formula [cf. Eq. (1)] applied to T2K.

small, which implies the approximation adopted in the effective θ_{13} could make a difference only in experiments with very high event numbers (i.e. very small statistical uncertainties) as well as correspondingly very small systematic uncertainties. More explicitly, if we assume the difference is about 2% as a typical value indicated in Fig. 4, then the total event number N_{tot} should be (according to $1/\sqrt{N_{\text{tot}}} \sim 2\%$) larger than $\mathcal{O}(10^3)$ to distinguish between the two curves. Current on-going accelerator neutrino experiments such as T2K, MINOS, NO ν A cannot reach such high statistics while the future experiment DUNE experiment will do so (861 ν_e events and 167 $\bar{\nu}_e$ events for 4 years of running [20]). However, the above requirement does not take the energy resolution into account (i.e. assumes no uncertainty in the energy measurement). Since the areas under the two curves are the same (by definition), the energy resolution has to be very high to see any differences between the two curves. The horizontal differences are typically around $\mathcal{O}(1\%)$, which implies that the energy resolution should reach $\Delta E_\nu/E_\nu < \mathcal{O}(1\%)$ to distinguish between them. Therefore, we can draw the conclusion that the approximation in the effective θ_{13} should be valid for experiments with $N_{\text{tot}} < \mathcal{O}(10^3)$ or $\Delta E_\nu/E_\nu > \mathcal{O}(1\%)$.

IV. PHENOMENOLOGICAL APPLICATIONS

As we have shown that our effective θ_{13}^{eff} can accurately describe the constraints from accelerator neutrino appearance data, in this section we shall apply this framework to phenomenological studies in what regards the determination and correlation of δ_{CP} , θ_{13} , θ_{23} and the mass ordering [31–36].

Since θ_{13} and θ_{23} can be measured independently in (anti)neutrino disappearance experiments and the measurements will be frequently used in this section, we list the recent results in Tab. II. The NO ν A measurement [12] of θ_{23} contains two best-fit solutions. Henceforth we will refer to the two solutions in the $\theta_{23} < 45^\circ$ and $\theta_{23} > 45^\circ$ octants as NO ν A $^-$ and NO ν A $^+$, respectively³. As future data will pin down the true values, it is of interest here to analyze the impact of the possible true values on the current and possible future hints of mass ordering and CP phase.

Table II. Recent measurements of θ_{13} and θ_{23} . N and I stand for the normal and inverted mass ordering respectively.

	Daya Bay [8]	RENO [9]	Double Chooz [10]
$\sin^2 2\theta_{13}$	0.0841 ± 0.0033	0.088 ± 0.011	0.111 ± 0.018
$\theta_{13}/^\circ$	$8.43^{+0.17}_{-0.17}$	$8.62^{+0.54}_{-0.57}$	$9.73^{+0.79}_{-0.85}$
	T2K [11]	NO ν A $^-$ [12]	NO ν A $^+$ [12]
$\sin^2 \theta_{23}$ (N)	$0.532^{+0.046}_{-0.068}$	$0.404^{+0.030}_{-0.022}$	$0.624^{+0.022}_{-0.030}$
$\theta_{23}/^\circ$ (N)	$46.8^{+2.7}_{-3.9}$	$39.5^{+1.7}_{-1.3}$	$52.2^{+1.3}_{-1.8}$
$\sin^2 \theta_{23}$ (I)	$0.534^{+0.043}_{-0.066}$	$0.398^{+0.030}_{-0.022}$	$0.618^{+0.022}_{-0.030}$
$\theta_{23}/^\circ$ (I)	$46.9^{+2.5}_{-3.8}$	$39.1^{+1.8}_{-1.3}$	$51.8^{+1.3}_{-1.8}$

³ With the leading term in the muon-neutrino survival probability proportional to $\sin^2 2\theta_{23}$, solutions in both octants are naturally expected.

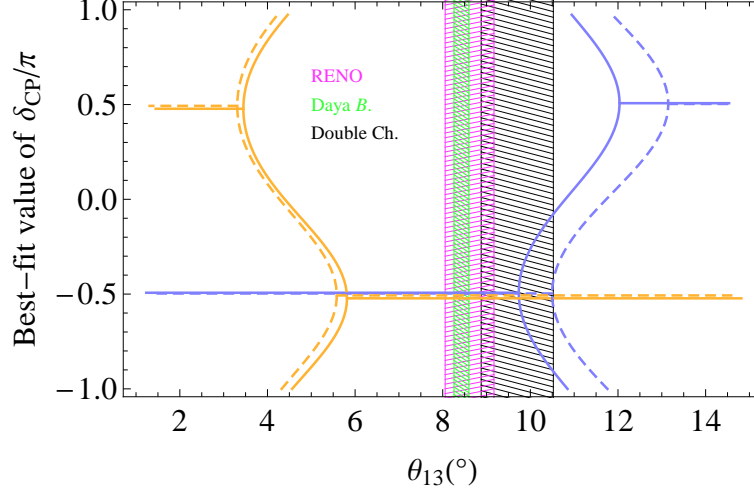


Figure 5. The best-fit value of δ_{CP} from T2K ν_e (blue curve) and $\bar{\nu}_e$ (orange curve) data [4] as a function of θ_{13} . Solid/dashed curves are for normal/inverted mass ordering. For $5.8^\circ < \theta_{13} < 9.7^\circ$, both ν_e and $\bar{\nu}_e$ data prefer a maximal CP violation value ($-\pi/2$) of δ_{CP} .

A. Analytical discussion

From the definition of effective θ_{13}^{eff} given in Eq. (5) we can obtain some conclusions analytically. Since the CP -even term and the α^2 term are much smaller than the other terms, we neglect them in the following discussion (they are taken into account in numerical calculations):

$$\frac{1}{2}S^2 \equiv \frac{1}{2}\sin^2 2\theta_{13}^{\text{eff}} \approx s_{23}^2 \sin^2 2\theta_{13} - 8\alpha J_{CP} f_s. \quad (26)$$

For fixed values of θ_{13} , θ_{23} and θ_{12} , S^2 has a maximum S_{max}^2 and a minimum S_{min}^2 at $\delta_{CP} = -\pi/2$ and $\pi/2$, respectively. If the measured value of S^2 falls into the range of $(S_{\text{min}}^2, S_{\text{max}}^2)$, then one can compute the corresponding value of $\sin \delta_{CP}$ by

$$\sin \delta_{CP} = \frac{2\sin^2 2\theta_{13}s_{23}^2 - S^2}{2\alpha f_s c_{13} \sin 2\theta_{12} \sin 2\theta_{13} \sin 2\theta_{23}}. \quad (27)$$

If the measured S^2 is not in the range $(S_{\text{min}}^2, S_{\text{max}}^2)$, then there may be a tension between the ν_e ($\bar{\nu}_e$) appearance and disappearance data. In this case, if these data are combined the best-fit value of δ_{CP} will be pushed to $\pm\pi/2$. Neglecting possible tensions, from the measurement of S^2 in ν_e ($\bar{\nu}_e$) appearance experiments one can obtain a CP -dependent measurement of θ_{13} , which is

$$\sin 2\theta_{13} \approx \frac{\beta \sin \delta_{CP} + \sqrt{2s_{23}^2 S^2 + \beta^2 \sin^2 \delta_{CP}}}{2s_{23}^2}, \quad \text{where } \beta \equiv \alpha f_s c_{13} \sin 2\theta_{12} \sin 2\theta_{23}. \quad (28)$$

Although the measurement is CP -dependent, since $-1 \leq \sin \delta_{CP} \leq 1$, θ_{13} measured in ν_e ($\bar{\nu}_e$) appearance experiments should be in the following range:

$$\frac{\sqrt{2s_{23}^2 S^2 + \beta^2} - |\beta|}{2s_{23}^2} \lesssim \theta_{13} \lesssim \frac{\sqrt{2s_{23}^2 S^2 + \beta^2} + |\beta|}{2s_{23}^2}. \quad (29)$$

Again, if the measurement of θ_{13} from reactor neutrinos is lower (or higher) than the lower (or upper) bound in Eq. (29), then the combined data fitting always prefers maximal CP violating values of δ_{CP} .

In Fig. 5, we show the best-fit value of δ_{CP} from the T2K ν_e ($\bar{\nu}_e$) appearance data, which confirms the above arguments. The χ^2 -function of δ_{CP} is obtained by

$$\chi_{\theta \text{ fixed}}^2(\delta_{CP}) = \chi^2 [S^2(\delta_{CP})|_{\theta \text{ fixed}}], \quad (30)$$

Table III. Parameters in the χ^2 -function (9) for the T2K data.

	ν_e normal	ν_e inverted	$\bar{\nu}_e$ normal	$\bar{\nu}_e$ inverted
n	32	32	4	4
k	1.86×10^2	51.5	1.55×10^2	55.9
b	4.8	5.4	2.5	2.5

where “ θ fixed” means that θ_{13} , θ_{23} and θ_{12} are fixed at given values (in particular $\theta_{23} = 46.6^\circ$, $\theta_{12} = 33.4^\circ$). The χ^2 -function of $S^2 \equiv \sin^2 2\theta_{13}^{\text{eff}}$ is given by Eq. (9), where n , b and k are listed in Tab. III for the T2K data.

Note that the observed number of 32 ν_e (or 4 $\bar{\nu}_e$) events is larger (or smaller) than the expected number, which should be 28.7 (6.0), 24.2 (6.9), or 19.6 (7.7) for $\delta_{CP} = -\pi/2$, 0, or $\pi/2$, respectively [37]. Since the expected number of ν_e ($\bar{\nu}_e$) decreases (or increases) with $\sin \delta_{CP}$, both the excess of observed ν_e and the deficit of $\bar{\nu}_e$ favor minimal $\sin \delta_{CP}$, i.e. $\delta_{CP} = -\pi/2$.

Using Eq. (30) and the values in Tab. III, we compute the best-fit value of δ_{CP} for both neutrino and antineutrino data, normal and inverted mass ordering, plotted by blue and orange, solid and dashed curves in Fig. 5 respectively. As shown in the plot, the T2K ν_e data favors a range of θ_{13} in $[9.7^\circ, 12.0^\circ]$ for the normal ordering or $[10.4^\circ, 13.1^\circ]$ for the inverted ordering. Currently reactor neutrino experiments including Daya Bay [8], RENO [9] and Double Chooz [10] all have measured smaller values of θ_{13} , marked by green, magenta and black bands (1σ CL) in Fig. 5. Therefore when the T2K ν_e data is combined with any of the reactor measurements, the best-fit value of δ_{CP} will necessarily become about $-\pi/2$. For the T2K $\bar{\nu}_e$ data, the favored range is $[3.4^\circ, 5.8^\circ]$ (normal) or $[3.9^\circ, 6.2^\circ]$ (inverted), which is smaller than the reactor measurements. So combining the T2K $\bar{\nu}_e$ data with any of the reactor measurements also leads to about $-\pi/2$ for the best-fit value of δ_{CP} . Note that due to corrections from the CP -even term, the actual value deviates from $-\pi/2$ by about $\mathcal{O}(0.01\pi)$.

B. Correlation of θ_{13} and δ_{CP}

If we regard $\sin^2 2\theta_{13}^{\text{eff}}$ as a function of $(\theta_{13}, \delta_{CP})$, then the χ^2 -function of $\sin^2 2\theta_{13}^{\text{eff}}$ can be straightforwardly converted into a χ^2 -function for a two-parameter fit in $(\theta_{13}, \delta_{CP})$ space. By allowing $\Delta\chi^2 \leq 2.3$ in the fit, we can produce 68% CL constraints on $(\theta_{13}, \delta_{CP})$ from the T2K ν_e and $\bar{\nu}_e$ appearance data, as shown by the blue (for ν_e) and orange (for $\bar{\nu}_e$) regions in the left panel of Fig. 6. The regions within solid (dashed) lines assume normal (inverted) mass ordering.

As we can expect from Eq. (26), which shows the dependence of $\sin^2 2\theta_{13}^{\text{eff}}$ on $\sin \delta_{CP}$, the orange and blue bounds all have the shapes of sine curves. The curves of ν_e and $\bar{\nu}_e$ are bent to opposite directions: the ν_e curves have minimal θ_{13} at $\delta_{CP} \approx -\pi/2$, while for $\bar{\nu}_e$ it is maximal. As a result, the orange region and the blue region have some overlap where δ_{CP} is mainly negative. This implies that combined fitting of ν_e and $\bar{\nu}_e$ appearance data favors negative δ_{CP} . In the plots we also show the 1σ CL bounds on θ_{13} from reactor neutrino experiments. When θ_{23} is fixed at 41° , the bounds from Daya Bay [8] and RENO [9] are below the overlap of the T2K ν_e and $\bar{\nu}_e$ constraints while the Double Chooz bound [10] is well compatible with the ν_e - $\bar{\nu}_e$ overlap. However, one should notice that this depends on the value of θ_{23} . If θ_{23} is fixed at the $\text{NO}\nu\text{A}^+$ value, as shown in the lower plots in Fig. 6, the ν_e - $\bar{\nu}_e$ overlap covers all the reactor bounds.

In the right panel of Fig. 6, we combine the T2K data with reactor neutrino data by

$$\chi^2(\theta_{13}, \delta_{CP}) = \chi_{\text{reactor}}^2(\theta_{13}) + \chi_{\text{T2K}}^2(S_{\nu_e}^2(\theta_{13}, \delta_{CP})) + \chi_{\text{T2K}}^2(S_{\bar{\nu}_e}^2(\theta_{13}, \delta_{CP})), \quad (31)$$

where the first, second and last terms are constraints from reactor neutrino data, T2K ν_e and $\bar{\nu}_e$ data, respectively. The χ^2 -functions of $S_{\nu_e}^2$ and $S_{\bar{\nu}_e}^2$ are given by Eq. (9) with (n, b, k) given in Tab. III. The χ^2 -function of θ_{13} from reactor neutrino data we adopt is

$$\chi_{\text{reactor}}^2(\theta_{13}) = \left(\frac{\sin^2 2\theta_{13} - \sin^2 2\theta_{13}^0}{\sigma_{13}} \right)^2. \quad (32)$$

Note that Eq. (32) assumes the distribution of $\sin^2 2\theta_{13}$ to be Gaussian with a central value $\sin^2 2\theta_{13}^0$ and the standard deviation σ_{13} given in Tab. II.

For each reactor neutrino experiment listed in Tab. II, we perform a χ^2 -fit combined with the T2K data and compute the corresponding 68% CL constraints on $(\theta_{13}, \delta_{CP})$, presented in the right panel of Fig. 6 by the green, magenta, and black contours (dashed for inverted mass ordering) for Daya Bay, RENO and Double Chooz, respectively. For all three reactor neutrino experiments the results favor negative δ_{CP} . Note that the significance depends on θ_{23} : when

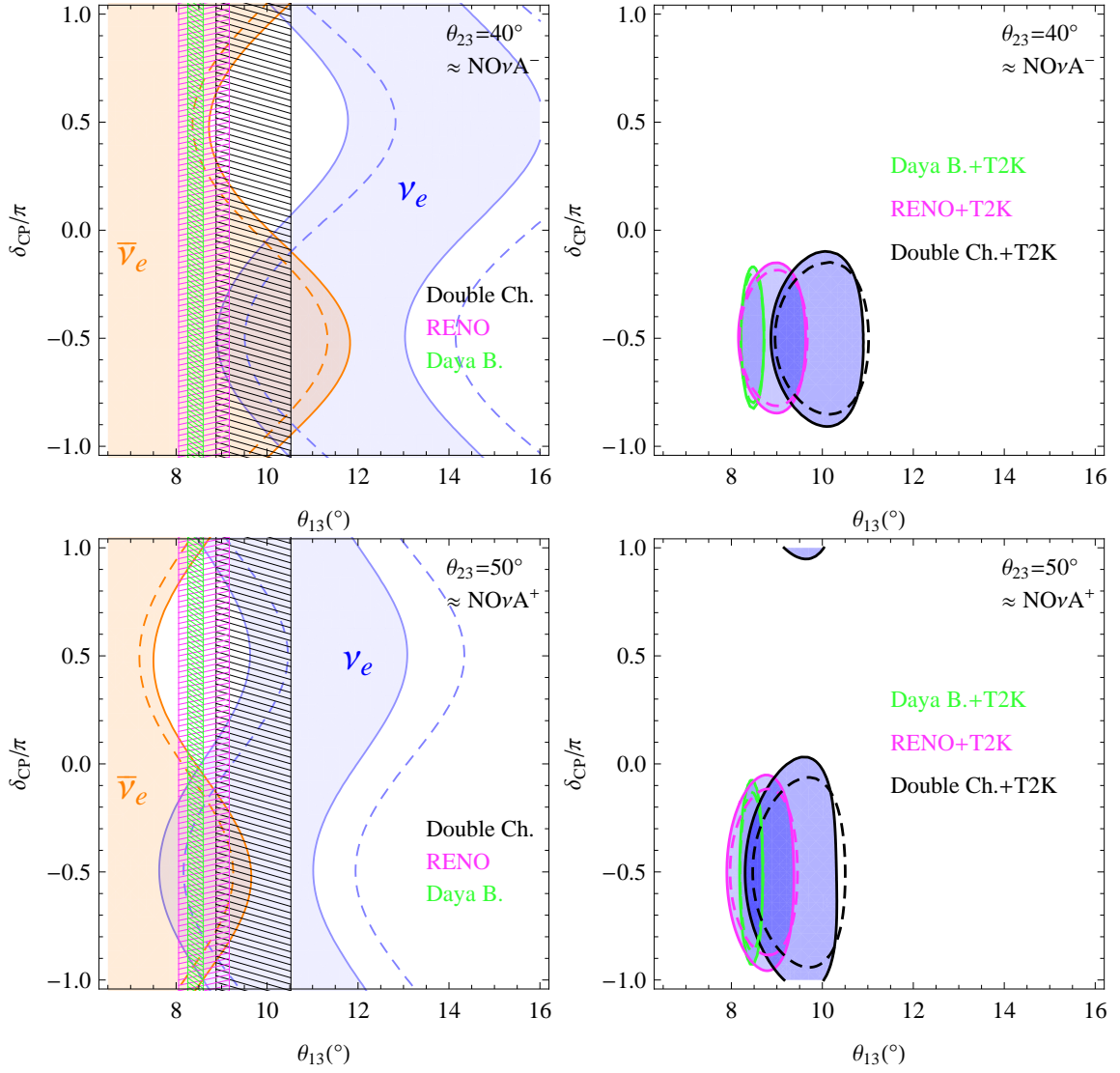


Figure 6. *Left panel:* constraints on $(\theta_{13}, \delta_{CP})$ from T2K [4] and constraints on θ_{13} from reactor neutrino experiments. Solid/dashed curves are for normal/inverted mass ordering, blue/orange curves for $\nu_e/\bar{\nu}_e$ appearance data, respectively. *Right panel:* Fit results on $(\theta_{13}, \delta_{CP})$ when T2K neutrino and antineutrino data are combined with reactor data. The upper plots apply for the $\text{NO}\nu\text{A}^-$ solution of θ_{23} , the lower plots for $\text{NO}\nu\text{A}^+$.

θ_{23} increases, the bounds on δ_{CP} expand and the significance of CP violation decreases. One finds from the plot that the influence of the true value of θ_{13} is not dramatic but still noteworthy; for θ_{23} in the second octant ($\text{NO}\nu\text{A}^+$) the effect is however slightly larger (note that in Fig. 6 the overlap regions of neutrino and antineutrino appearance data fits in this case better with the reactor determinations of θ_{13}). The origin of this behavior is easy to identify in Eq. (4), where $\sin^2 \theta_{23}$ appears. Hence, a value of θ_{23} in the upper octant may thus reduce the current significance of the hints for maximal CP violation.

C. Correlation of θ_{23} and δ_{CP}

As we have seen, θ_{23} also plays an important role in the measurement of δ_{CP} in accelerator neutrino experiments. Thus we shall study the relation of δ_{CP} and θ_{23} in more detail. Similar to Eq. (31), we have the following combined χ^2 -function:

$$\chi^2(\theta_{23}, \delta_{CP}) = \chi_{\text{Acc. Dis.}}^2(\theta_{23}) + \chi_{\text{T2K}}^2(S_{\nu_e}^2(\theta_{23}, \delta_{CP})) + \chi_{\text{T2K}}^2(S_{\bar{\nu}_e}^2(\theta_{23}, \delta_{CP})). \quad (33)$$

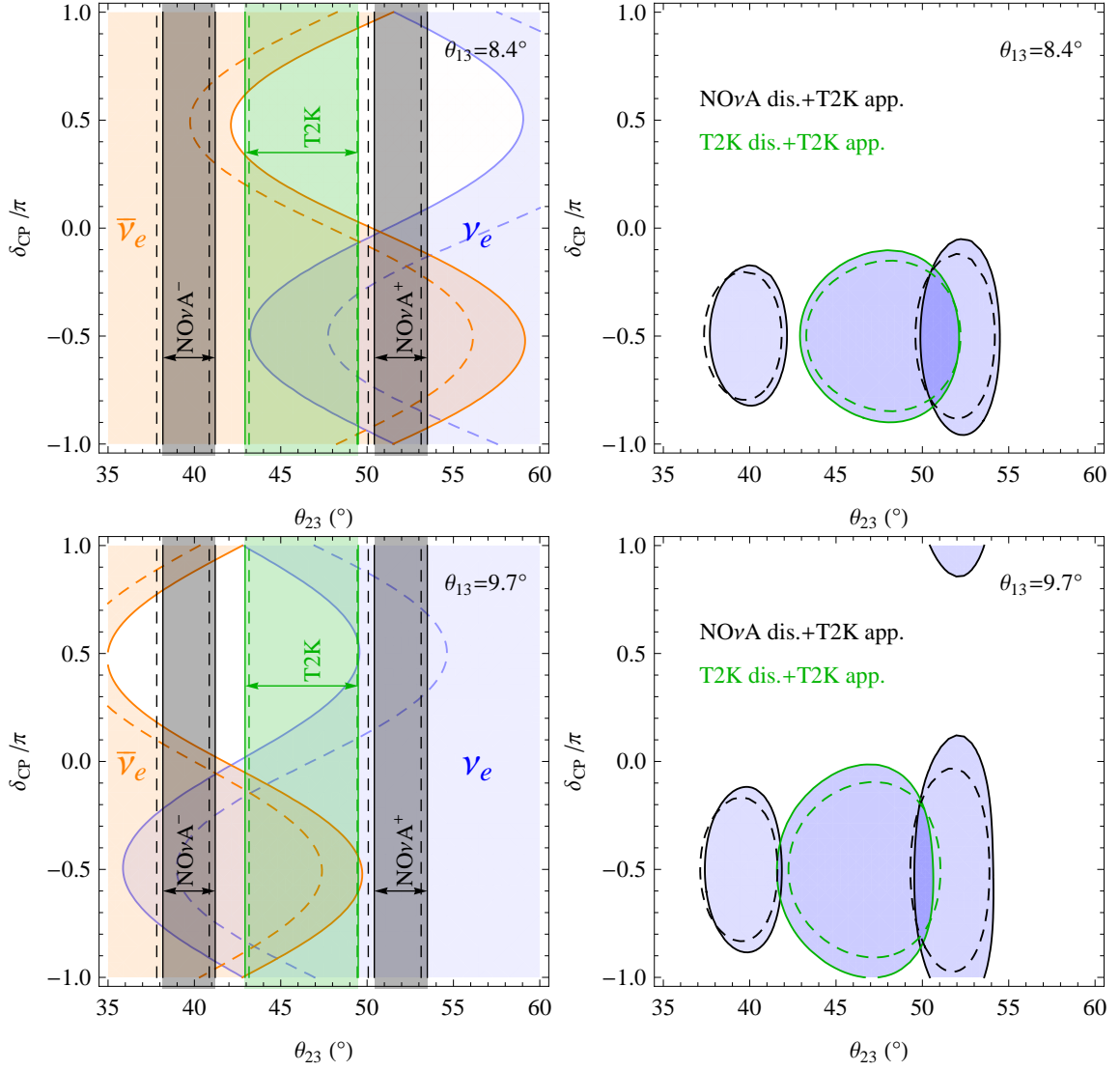


Figure 7. Constraints on $(\theta_{23}, \delta_{CP})$ from T2K appearance data combined with ν_μ disappearance data from T2K and NO ν A. Solid/dashed curves are for normal/inverted mass ordering, blue/orange curves for $\nu_e/\bar{\nu}_e$ appearance data, respectively. The upper plots are for the best-fit value of θ_{13} from Daya Bay/RENO, the lower ones for the best-fit value of θ_{13} from Double Chooz.

Here $\chi_{\text{Acc. Dis.}}^2$ denotes the χ^2 -function of θ_{23} constrained by accelerator neutrino disappearance experiments. In Tab. II, we list the measurements of θ_{23} from T2K and NO ν A. For simplicity, in $\chi_{\text{Acc. Dis.}}^2$ we assume a Gaussian distribution of $\sin^2 \theta_{23}$,

$$\chi_{\text{Acc. Dis.}}^2(\theta_{23}) = \left(\frac{\sin^2 \theta_{23} - \sin^2 \theta_{23}^0}{\sigma_{23}} \right)^2, \quad (34)$$

where σ_{23} is taken as the mean value of the upper and lower uncertainties. In the left panel of Fig. 7, we show separate constraints on $(\delta_{CP}, \theta_{23})$ from the three terms in Eq. (33). The constraints from the T2K ν_e and $\bar{\nu}_e$ appearance data are presented by blue and orange regions. We can explain this behavior by rewriting Eq. (26) as

$$s_{23}^2 \approx \frac{S^2}{2 \sin^2 2\theta_{13}} + \frac{\beta}{\sin 2\theta_{13}} \sin \delta_{CP}, \quad (35)$$

where β has been defined in Eq. (28). Although β contains $\sin 2\theta_{23}$, for $40^\circ < \theta_{23} < 50^\circ$, the dependence of β on θ_{23} is very weak ($0.985 \leq \sin 2\theta_{23} \leq 1$) so one can approximately treat it as a constant with respect to θ_{23} . Therefore

Eq. (35) shows that the constraints on s_{23}^2 from the ν_e and $\bar{\nu}_e$ appearance data are δ_{CP} dependent and the dependence is described by a NLO correction proportional to $\sin \delta_{CP}$. Because β in Eq. (35) has opposite signs for ν_e and $\bar{\nu}_e$, the curves are bent to opposite directions so that the blue and orange regions have overlap around $\delta = -\pi/2$. The overlap can be approximately regarded as the region of preferred values of $(\delta_{CP}, \theta_{23})$ by the T2K appearance data. Note that this region depends on the fixed value of θ_{13} used in Eq. (33). We choose two values $\theta_{13} = 8.4^\circ$ and $\theta_{13} = 9.7^\circ$ (which are the central values of the Daya Bay/RENO and Double Chooz measurements, respectively) to draw the plots in Fig. 7. For both cases, θ_{23} measured from the T2K ν_μ ($\bar{\nu}_\mu$) disappearance experiment (the green band) is well compatible with the appearance data. The NO ν A disappearance data favor non-maximal θ_{23} , showing two separate 1σ bands (black) on the plots. For $\theta_{13} = 8.4^\circ$, the band of NO ν A $^+$ is well compatible with the T2K appearance data while the other band NO ν A $^-$ is not. However, for $\theta_{13} = 9.7^\circ$, the preference moves to the band in the lower octant. In the right panel of Fig. 7 we show 1σ constraints from a combined fit. For the combination of the T2K disappearance data with the appearance data, the 1σ bound of δ_{CP} is $(-0.9\pi, -0.1\pi)$ when θ_{13} is fixed at 8.4° and it expands to $(-1.0\pi, -0.0\pi)$ if θ_{13} is fixed at 9.7° . The combination of the NO ν A disappearance data with T2K appearance data, however, is more sensitive to the value of θ_{13} . When θ_{13} is 8.4° , the two separate regions in black contours have δ_{CP} limited in $(-0.8\pi, -0.2\pi)$ or $(-0.9\pi, -0.1\pi)$. When θ_{13} is increased to 9.7° , both expand by about 0.1π or 0.2π .

One finds from the plot that the influence of the true value of θ_{13} is not dramatic but nevertheless noteworthy; if θ_{13} takes the large value, the effect of θ_{23} from NO ν A $^+$ is however slightly larger (note that in Fig. 7 the overlap regions of neutrino and antineutrino appearance data fit in this case show a slight tension with the NO ν A $^+$ solution). Hence, if θ_{23} lies in the second octant and θ_{13} is large (i.e. given by value of Double Chooz), then the significance of the hints for maximal CP violation is reduced.

D. Discovery of CP violation in the near future

The current ν_e and $\bar{\nu}_e$ data of T2K, which was collected from 2010 to 2016 with 1.5×10^{21} protons-on-target (POT), shows only a moderate hint for CP Violation (CPV). Here we will investigate how this might increase with future data (see also [38, 39]). The T2K experiment will keep on collecting data until 2026 and will obtain more than 10 times data (20×10^{21} POT) [40], before the next generation of accelerator neutrino experiments (e.g. DUNE [20], T2HK [21] or T2HKK [41]) takes over.

To study this issue, we use the following χ^2 -function to compute the pre-DUNE significance of CPV in the data:

$$\chi_{\text{CPV}}^2(\theta_{23}, \theta_{13}) = \min_{\delta_{CP}=0 \text{ or } \pi} [\chi_{\nu_e+\bar{\nu}_e}^2(\theta_{23}, \theta_{13}, \delta_{CP})] - \min_{\delta_{CP} \in [-\pi, \pi]} [\chi_{\nu_e+\bar{\nu}_e}^2(\theta_{23}, \theta_{13}, \delta_{CP})], \quad (36)$$

where $\chi_{\nu_e+\bar{\nu}_e}^2$ is the sum of the χ^2 -functions of the ν_e and $\bar{\nu}_e$ data. Our definition χ_{CPV}^2 is the difference of how good a fit with CP conservation is with respect to the CP violating best-fit value. For the future data of T2K collected until 2026, we take the estimated numbers from Ref. [40] for the normal mass ordering, including 558.7 ν_e events and 115.8 $\bar{\nu}_e$ events, with a background of 110.1 (ν_e)+63.5 ($\bar{\nu}_e$) events. These numbers are assuming maximal CP violation ($\delta_{CP} = -\pi/2$) and equal exposure in the neutrino and antineutrino modes, i.e. 1.0×10^{22} POT for ν_e and 1.0×10^{22} for $\bar{\nu}_e$. We will refer to this data as T2K 2026 (1 : 1). It may be favorable however to have different ratios of neutrino and antineutrino data. Hence, we also analyze the cases (1 : 2) and (2 : 1). These can be studied by rescaling the event numbers of the (1 : 1) mode.

The results are presented in Fig. 8, where we show the significance of CPV in both the current data (T2K 2016) and the future data (T2K 2026) with three different exposure ratios, (1 : 1), (1 : 2) and (2 : 1). As we can see, compared to the T2K 2016 data, the future data will have more enhanced sensitivity on CPV. Changing the exposure ratio can affect the result. However whether this increases or decreases the significance of CPV depends on values of θ_{13} and θ_{23} . For example, if $\theta_{13} = 8.43^\circ$ and $\theta_{23} = 46.8^\circ$, which are the best-fit values of Daya Bay and T2K disappearance measurements, then the (2 : 1) mode could reach 4.8σ significance of CPV (cf. Tab. IV), better than the (1 : 1) and (1 : 2) modes which have 4.4σ and 3.9σ respectively. If θ_{23} is changed to the best-fit value of NO ν A $^+$, ($\theta_{23} = 52.5^\circ$), then the (1 : 2) mode could reach 2.5σ , larger than 2.3σ and 2.2σ in the (1 : 1) and (2 : 1) mode.

At first sight it may be surprising that more neutrino data is helping the significance of CP violation, rather than an equal share of more antineutrino data. The reason is that the antineutrino channel has a lower event rate (about 1/5 of the neutrino channel) and a higher background (about 1:1 signal-to-background ratio, 4 times higher than the neutrino channel) [40].

To sum up, there is optimization potential for the CP phase in future data taking. Given the large theoretical significance and interest of a maximal CP phase (see Refs. [42–63] for an incomplete list), this could be worth exploring further. We note that since δ_{CP} is expected to receive the largest model corrections to any neutrino oscillation parameter [64], a value close to a special one like $-\pi/2$ is a strong hint that a symmetry protects this special value, and thus truly a worthwhile measurement.

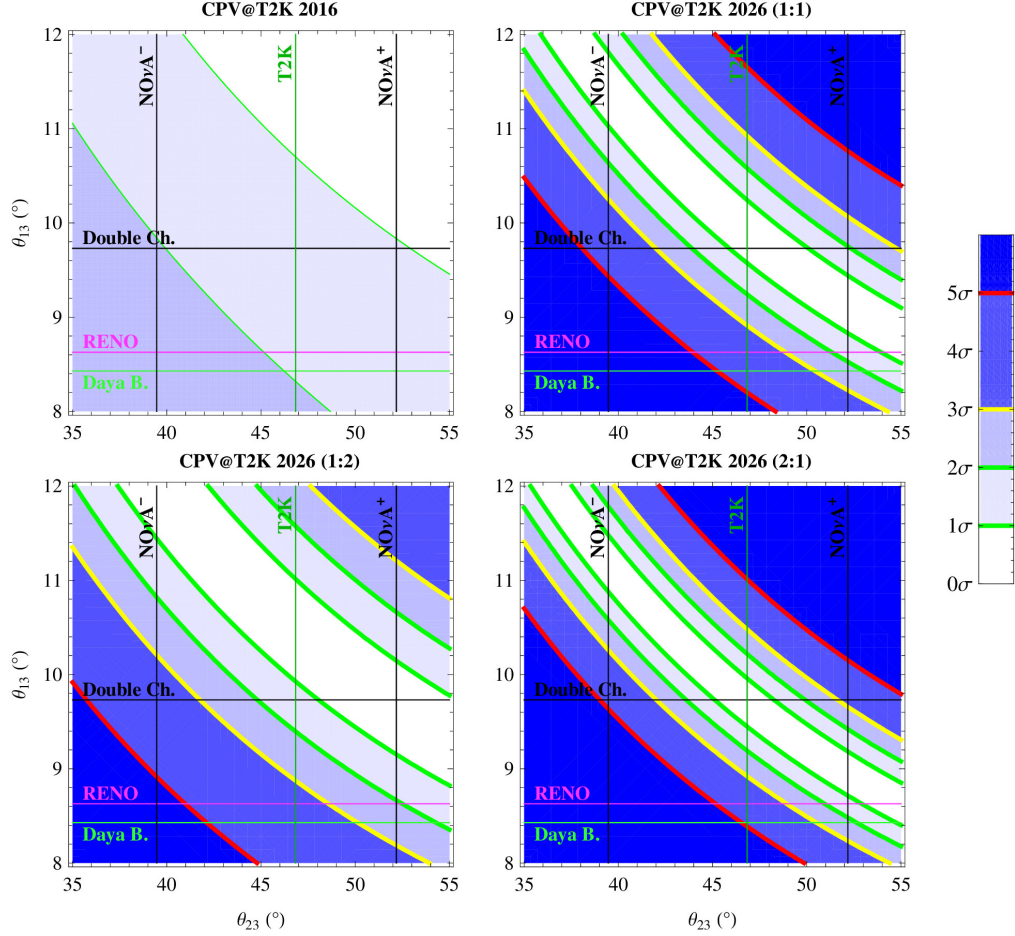


Figure 8. CP violation (CPV) in T2K data. *Upper left panel*: current significance of CPV in T2K (data collected until May 2016 with 1.5×10^{21} POT [4]). *Other panels*: future sensitivities of CPV with 20×10^{21} POT [40] assuming $\delta_{CP} = -\pi/2$. The ratios [e.g. (1 : 2), (2 : 1)] denote ratios of running times in neutrino and antineutrino modes.

Table IV. Significance of CP violation in current and future T2K. The four numbers in each bracket stand for the significance (in the unit of standard deviation σ) of CPV in the data of T2K2016, T2K2026 (1 : 1), T2K2026 (1 : 2) and T2K2026 (2 : 1), respectively, assuming that the true values of θ_{23} and θ_{13} are fixed at different best-fit values.

	$\theta_{23} = 39.5^\circ$ (NO νA^-)	$\theta_{23} = 46.8^\circ$ (T2K)	$\theta_{23} = 52.2^\circ$ (NO νA^+)
$\theta_{13} = 9.73^\circ$ (Double Ch.)	(2.0, 4.3, 3.8, 4.7)	(1.5, 0.5, 1.4, 0.1)	(1.1, 1.9, 0.2, 3.3)
$\theta_{13} = 8.62^\circ$ (RENO)	(2.3, 6.7, 5.4, 7.8)	(1.9, 3.8, 3.5, 4.1)	(1.6, 1.7, 2.1, 1.4)
$\theta_{13} = 8.43^\circ$ (Daya B.)	(2.4, 7.0, 5.6, 8.2)	(2.0, 4.4, 3.9, 4.8)	(1.7, 2.3, 2.5, 2.2)

E. The mass ordering

Finally, we would like to study the current sensitivity on the mass ordering. Here the much harder to analyze atmospheric neutrino data has large impact⁴, our focus lies however just on ν_e and $\bar{\nu}_e$ appearance data. In the not so far future, ORCA [66] and PINGU [67] are also expected to contribute to the issue, and JUNO [68] will settle the question on the mass ordering with a very different method than the one based on matter effects.

⁴ We note that completely independent cosmology data has, depending on used data sets, also some preference for the normal ordering, see e.g. [65].

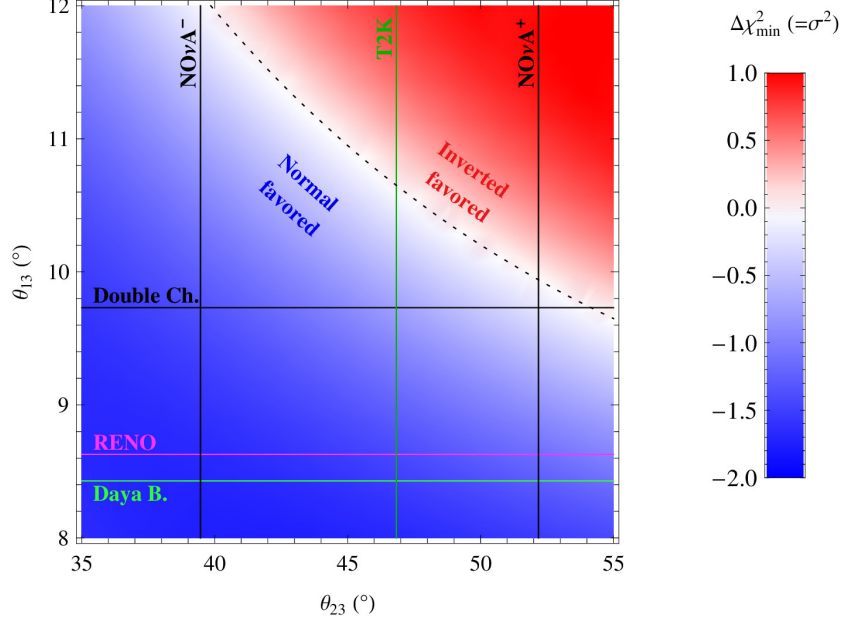


Figure 9. Comparison of normal and inverted mass ordering by $\Delta\chi^2_{\min} \equiv \chi^2_{\min N} - \chi^2_{\min I}$ from T2K appearance data. The black dotted curve corresponds to $\Delta\chi^2_{\min} = 0$. With the one-parameter fitting performed here, $\Delta\chi^2_{\min} = \sigma^2$.

We compare the normal and inverted cases by their minimal χ^2 -values,

$$\Delta\chi^2_{\min} \equiv \chi^2_{\min N} - \chi^2_{\min I}, \quad (37)$$

where the subscript “N” or “I” stands for normal or inverted ordering respectively; “min” stands for the minimization over the unknown parameter δ_{CP} . More explicitly, χ^2_{\min} above is computed by

$$\chi^2_{\min}(\theta_{23}, \theta_{13}) = \min_{\delta_{CP}} [\chi^2_{\nu_e}(\theta_{23}, \theta_{13}, \delta_{CP}) + \chi^2_{\bar{\nu}_e}(\theta_{23}, \theta_{13}, \delta_{CP})],$$

for any given values of θ_{23} and θ_{13} . Here $\chi^2_{\nu_e}$ and $\chi^2_{\bar{\nu}_e}$ are constraints from the T2K ν_e and $\bar{\nu}_e$ appearance data respectively, computed according to Tab. I and Tab III. The result is shown in Fig. 9, where the blue region has $\chi^2_{\min N} < \chi^2_{\min I}$, which means NO is favored over IO by the T2K appearance data while in the red region IO is more favored. We also show the boundary where $\Delta\chi^2_{\min} = 0$ by the black dotted curve. Fig. 9 implies that except for large θ_{13} and θ_{23} , the T2K appearance data prefer NO over IO. This can also be confirmed in Fig. 6 or Fig. 7, where the overlap of the orange and blue regions becomes smaller when the mass ordering is changed from NO to IO.

We see from Fig. 9, however, that within the expected values of θ_{23} and θ_{13} the significance of any mass ordering can vary by about one standard deviation.

V. CONCLUSION

Some attention has recently been cast on hints for a nontrivial CP phase and the normal mass ordering. Since the combination of reactor and accelerator neutrino measurements is the origin of this we revisit the crucial parameter correlations in oscillation probabilities. Noting the different available central values of θ_{13} and θ_{23} from the different reactor and long-baseline experiments, we performed an analysis on their impact of the ranges of the CP phase and the preference of the mass ordering. While surely not a global fit including all available data, some new insights have been obtained.

To facilitate comparison of reactor and accelerator data, we have proposed the effective θ_{13}^{eff} , which is defined in Eq. (5). We have demonstrated that the effective θ_{13}^{eff} can reproduce the reported constraint on δ_{CP} and θ_{13} by the T2K collaboration very well. It can furthermore straightforwardly explain why future long-baseline experiments will be more sensitive to the CP phase when δ_{CP} is around zero, rather than when it is around $-\pi/2$.

The effective θ_{13}^{eff} can be applied to phenomenological studies of reactor and accelerator neutrino measurements. Optimization potential for the determination of δ_{CP} around the theoretically highly interesting value $-\pi/2$ is discussed. Moreover, using the different available best-fit values of θ_{13} and θ_{23} from reactor experiments and from T2K/NO ν A, respectively, we studied their impact on the current ranges of δ_{CP} and the mass ordering. We have shown that, depending on the true values of θ_{13} and θ_{23} , the current sensitivities are subject to change.

We hope that our study prompts some discussion on the robustness of existing hints (or any future hints) in the data, and contributes to future discussion of neutrino oscillation results.

ACKNOWLEDGMENTS

WR is supported by the DFG with grant RO 2516/6-1 in the Heisenberg program.

-
- [1] K. Abe *et al.* (T2K Collaboration), Phys.Rev.Lett. **112**, 061802 (2014), arXiv:1311.4750 [hep-ex].
 - [2] J. Bian (NO ν A), in *Proceedings, Meeting of the APS Division of Particles and Fields (DPF 2015): Ann Arbor, Michigan, USA, 4-8 Aug 2015* (2015) arXiv:1510.05708 [hep-ex].
 - [3] K. Abe *et al.* (T2K), Phys. Rev. Lett. **118**, 151801 (2017), arXiv:1701.00432 [hep-ex].
 - [4] K. Abe *et al.* (T2K), (2017), arXiv:1707.01048 [hep-ex].
 - [5] F. Capozzi, E. Lisi, A. Marrone, D. Montanino, and A. Palazzo, Nucl. Phys. **B908**, 218 (2016), arXiv:1601.07777 [hep-ph].
 - [6] I. Esteban, M. C. Gonzalez-Garcia, M. Maltoni, I. Martinez-Soler, and T. Schwetz, JHEP **01**, 087 (2017), arXiv:1611.01514 [hep-ph].
 - [7] P. F. de Salas, D. V. Forero, C. A. Ternes, M. Tortola, and J. W. F. Valle, (2017), arXiv:1708.01186 [hep-ph].
 - [8] F. P. An *et al.* (Daya Bay), Phys. Rev. **D95**, 072006 (2017), arXiv:1610.04802 [hep-ex].
 - [9] H. Seo (RENO), *Proceedings, 14th International Conference on Topics in Astroparticle and Underground Physics (TAUP 2015): Torino, Italy, September 7-11, 2015*, J. Phys. Conf. Ser. **718**, 062053 (2016).
 - [10] T. Matsubara (Double Chooz), *Proceedings, 38th International Conference on High Energy Physics (ICHEP 2016): Chicago, IL, USA, August 3-10, 2016*, PoS **ICHEP2016**, 469 (2016).
 - [11] K. Abe *et al.* (T2K), Phys. Rev. **D96**, 011102 (2017), arXiv:1704.06409 [hep-ex].
 - [12] P. Adamson *et al.* (NO ν A), Phys. Rev. Lett. **118**, 151802 (2017), arXiv:1701.05891 [hep-ex].
 - [13] M. Freund, Phys.Rev. **D64**, 053003 (2001), arXiv:hep-ph/0103300 [hep-ph].
 - [14] A. Cervera, A. Donini, M. Gavela, J. Gomez Cadenas, P. Hernandez, *et al.*, Nucl.Phys. **B579**, 17 (2000), arXiv:hep-ph/0002108 [hep-ph].
 - [15] K. Olive *et al.* (Particle Data Group), Chin.Phys. **C38**, 090001 (2014).
 - [16] K. Abe *et al.* (T2K Collaboration), Phys.Rev.Lett. **111**, 211803 (2013), arXiv:1308.0465 [hep-ex].
 - [17] P. Adamson *et al.* (MINOS Collaboration), Phys.Rev.Lett. **106**, 181801 (2011), arXiv:1103.0340 [hep-ex].
 - [18] D. Ayres *et al.* (NO ν A Collaboration), (2004), arXiv:hep-ex/0503053 [hep-ex].
 - [19] R. Patterson (NO ν A Collaboration), Nucl.Phys.Proc.Suppl. **235-236**, 151 (2013), arXiv:1209.0716 [hep-ex].
 - [20] R. Acciarri *et al.* (DUNE), (2015), arXiv:1512.06148 [physics.ins-det].
 - [21] K. Abe *et al.* (Hyper-Kamiokande Working Group) (2014) arXiv:1412.4673 [physics.ins-det].
 - [22] L. Wolfenstein, Phys.Rev. **D17**, 2369 (1978).
 - [23] S. Mikheev and A. Y. Smirnov, Sov.J.Nucl.Phys. **42**, 913 (1985).
 - [24] S. Mikheev and A. Y. Smirnov, Nuovo Cim. **C9**, 17 (1986).
 - [25] X.-J. Xu, JHEP **10**, 090 (2015), arXiv:1502.02503 [hep-ph].
 - [26] K. Abe *et al.* (T2K Collaboration), Phys.Rev. **D88**, 032002 (2013), arXiv:1304.0841 [hep-ex].
 - [27] C. Andreopoulos *et al.*, Nucl. Instrum. Meth. **A614**, 87 (2010), arXiv:0905.2517 [hep-ph].
 - [28] N. Nath, M. Ghosh, and S. Goswami, Nucl. Phys. **B913**, 381 (2016), arXiv:1511.07496 [hep-ph].
 - [29] P. Ballett, S. F. King, S. Pascoli, N. W. Prouse, and T. Wang, Phys. Rev. **D96**, 033003 (2017), arXiv:1612.07275 [hep-ph].
 - [30] S. Fukasawa, M. Ghosh, and O. Yasuda, Nucl. Phys. **B918**, 337 (2017), arXiv:1607.03758 [hep-ph].
 - [31] H. Minakata, H. Sugiyama, O. Yasuda, K. Inoue, and F. Suekane, Phys. Rev. **D68**, 033017 (2003), [Erratum: Phys. Rev.D70,059901(2004)], arXiv:hep-ph/0211111 [hep-ph].
 - [32] P. Huber, M. Lindner, T. Schwetz, and W. Winter, Nucl. Phys. **B665**, 487 (2003), arXiv:hep-ph/0303232 [hep-ph].
 - [33] H. Minakata and H. Sugiyama, Phys. Lett. **B580**, 216 (2004), arXiv:hep-ph/0309323 [hep-ph].
 - [34] O. Mena and S. J. Parke, Phys. Rev. **D70**, 093011 (2004), arXiv:hep-ph/0408070 [hep-ph].
 - [35] A. Ghosh, T. Thakore, and S. Choubey, JHEP **04**, 009 (2013), arXiv:1212.1305 [hep-ph].
 - [36] S. Choubey and A. Ghosh, JHEP **11**, 166 (2013), arXiv:1309.5760 [hep-ph].
 - [37] L. Magaletti (T2K), *Proceedings, Neutrino Oscillation Workshop (NOW 2016): International Workshop on Neutrino and Astroparticle Physics (NOW 2016): Otranto (Lecce), Italy, September 4-11, 2016*, PoS **NOW2016**, 003 (2017).
 - [38] M. Ghosh, S. Goswami, and S. K. Raut, Mod. Phys. Lett. **A32**, 1750034 (2017), arXiv:1409.5046 [hep-ph].

- [39] M. Ghosh, Phys. Rev. **D93**, 073003 (2016), arXiv:1512.02226 [hep-ph].
- [40] K. Abe *et al.*, (2016), arXiv:1609.04111 [hep-ex].
- [41] K. Abe *et al.* (Hyper-Kamiokande proto-), (2016), arXiv:1611.06118 [hep-ex].
- [42] P. F. Harrison and W. G. Scott, Phys. Lett. **B547**, 219 (2002), arXiv:hep-ph/0210197 [hep-ph].
- [43] E. Ma, Phys.Rev. **D66**, 117301 (2002), arXiv:hep-ph/0207352 [hep-ph].
- [44] K. Babu, E. Ma, and J. Valle, Phys.Lett. **B552**, 207 (2003), arXiv:hep-ph/0206292 [hep-ph].
- [45] E. Ma, Mod.Phys.Lett. **A17**, 2361 (2002), arXiv:hep-ph/0211393 [hep-ph].
- [46] W. Grimus and L. Lavoura, Phys.Lett. **B579**, 113 (2004), arXiv:hep-ph/0305309 [hep-ph].
- [47] C. C. Nishi, Phys. Rev. **D88**, 033010 (2013), arXiv:1306.0877 [hep-ph].
- [48] E. Ma, Phys. Rev. Lett. **112**, 091801 (2014), arXiv:1311.3213 [hep-ph].
- [49] S. Fraser, E. Ma, and O. Popov, Phys. Lett. **B737**, 280 (2014), arXiv:1408.4785 [hep-ph].
- [50] G.-N. Li and X.-G. He, Phys. Lett. **B750**, 620 (2015), arXiv:1505.01932 [hep-ph].
- [51] E. Ma, A. Natale, and O. Popov, Phys. Lett. **B746**, 114 (2015), arXiv:1502.08023 [hep-ph].
- [52] A. Di Iura, C. Hagedorn, and D. Meloni, JHEP **08**, 037 (2015), arXiv:1503.04140 [hep-ph].
- [53] R. N. Mohapatra and C. C. Nishi, JHEP **08**, 092 (2015), arXiv:1506.06788 [hep-ph].
- [54] Y.-L. Zhou, (2014), arXiv:1409.8600 [hep-ph].
- [55] A. S. Joshipura and K. M. Patel, Phys. Lett. **B749**, 159 (2015), arXiv:1507.01235 [hep-ph].
- [56] H.-J. He, W. Rodejohann, and X.-J. Xu, Phys. Lett. **B751**, 586 (2015), arXiv:1507.03541 [hep-ph].
- [57] H.-J. He and X.-J. Xu, Phys. Rev. **D86**, 111301 (2012), arXiv:1203.2908 [hep-ph].
- [58] W. Rodejohann and X.-J. Xu, (2017), arXiv:1705.02027 [hep-ph].
- [59] W. Rodejohann and X.-J. Xu, Eur. Phys. J. **C76**, 138 (2016), arXiv:1509.03265 [hep-ph].
- [60] Z.-h. Zhao, (2017), arXiv:1703.04984 [hep-ph].
- [61] C. C. Nishi and B. L. Sanchez-Vega, JHEP **01**, 068 (2017), arXiv:1611.08282 [hep-ph].
- [62] P. Chen, G.-J. Ding, F. Gonzalez-Canales, and J. W. F. Valle, Phys. Lett. **B753**, 644 (2016), arXiv:1512.01551 [hep-ph].
- [63] T. Fukuyama, (2017), arXiv:1701.04985 [hep-ph].
- [64] W. Rodejohann and X.-J. Xu, Nucl. Phys. **B899**, 463 (2015), arXiv:1508.06063 [hep-ph].
- [65] S. Hannestad and T. Schwetz, JCAP **1611**, 035 (2016), arXiv:1606.04691 [astro-ph.CO].
- [66] S. Adrian-Martinez *et al.* (KM3Net), J. Phys. **G43**, 084001 (2016), arXiv:1601.07459 [astro-ph.IM].
- [67] M. G. Aartsen *et al.* (IceCube PINGU), (2014), arXiv:1401.2046 [physics.ins-det].
- [68] F. An *et al.* (JUNO), J. Phys. **G43**, 030401 (2016), arXiv:1507.05613 [physics.ins-det].